optica

Analyzing and generating multimode optical fields using self-configuring networks

David A. B. Miller

Ginzton Laboratory, Stanford University, 348 Via Pueblo Mall, Stanford, California 94305, USA (dabm@stanford.edu)

Received 27 February 2020; revised 10 May 2020; accepted 12 June 2020 (Doc. ID 391592); published 13 July 2020

Working with finite numbers of modes to describe, generate, and detect optical fields can be both mathematically economical and physically useful. Such a modal basis can map directly to various applications in communications, sensing, and processing. But, we need a way to generate and analyze such fields, including measurement and control of both the relative amplitudes and phases of the modal components. Ideally such an analysis scheme would operate directly on the field, without needing a separate, mutually coherent reference beam. Here, we show first how to measure all those relative amplitudes and phases automatically and simultaneously. The method repurposes a self-configuring network of 2 × 2 blocks, such as integrated Mach–Zehnder interferometers, that can automatically align itself to the optical field by a sequence of simple one-parameter power minimizations when network elements, such as phase shifters, are adjusted. The optical field is then directly deduced from the resulting settings of those elements. We show how the entire network can be calibrated for such measurements, automatically and with just two light beams. Then, using the same calibration and running the mesh backwards, we can also controllably generate an arbitrary multimode field. Explicit algorithms and formulas are given for operating this system.

https://doi.org/10.1364/OPTICA.391592

1. INTRODUCTION

Increasingly in optics, we exploit complex multimode light fields [1]—for example, in communications [2], classical and quantum linear optical information processing [3–5], and in various opportunities in adaptive systems for sensing and communications [6]. To extract complete optical information from multimode fields, we need to analyze the relative amplitude and phase of the different modes. Similarly, we want to be able to generate arbitrary multimode field inputs for linear computation and communication or for full control of an optical stimulus in sensing. Schemes based on single spatial light modulators (SLMs) have shown impressive performance in sequentially analyzing such multimode fields (e.g., [7,8]); a single SLM can also generate an arbitrary field, though generally with some inherent power loss. Other multiplane schemes based on several SLMs or fixed diffractive elements can simultaneously separate components of different specific modes from large multimode fields (e.g., [9,10]).

Though such separations can give the relative magnitudes of each mode, a full analysis also requires their relative phases. With some further measurements and processing in those schemes, full-field interferometry can analyze the full complex field [7]. To find the relative phase of all the components of a field, either as modes or pixels, we could interfere simultaneously with a known (and mutually coherent) reference field at a set of different phase shifts (see, e.g., [7]). We may not have such a mutually coherent reference field, however, when simply observing some incoming field. One solution in principle could use a cascade of interferometers that progressively establish the relative phases between all of the components (modes or pixels) of a field. Cascading multiple interferometers would have been quite challenging historically. Recently, however, complex interferometric networks have become possible, based on integrated arrays or meshes of waveguide Mach–Zehnder interferometers (MZIs), and, equally importantly, algorithms have emerged to control and configure such complex interferometric systems automatically [11–15]. Such meshes also allow efficient and adaptive separation and manipulation of multiple modes. Here, we exploit one such mesh approach, originally proposed to allow self-configuring automatic coupling of complex beams [13]. Because this kind of mesh gives exactly the kind of cascade of interferometers that we need, adding novel algorithms, we can repurpose it for automatically measuring or generating both the relative amplitudes and phases of such multimode fields, potentially even tracking changing inputs in real time [11,12]. Furthermore, we show how such an interferometric mesh can be calibrated automatically for these purposes, using just two simple light beams. Hence, we now have a simple progressive method for measuring full amplitudes and phases of an arbitrary multimode light field based only on that field itself.

The key idea of the measuring approach is that, once such a mesh has self-configured to align itself to an input beam or field [13,14], all of the information about the relative amplitudes and phases of the input beam is contained in the resulting settings—e.g., the phase shifts and/or coupling ratios of the interferometers.

Essentially, in this self-configuration, we have performed all of the relative interferometric measurements across all the input modes. The relative amplitudes and phases of the input field can then be deduced from those settings by simple arithmetic. Furthermore, by running such a mesh system backwards using a single source light beam injected "backwards" into the "output", any such multimode field can instead be controllably generated, emerging from the original "inputs."

The mesh itself operates on the field in its multiple different input (single-mode) waveguides. Such meshes could operate directly on a "free-space" optical input field by sampling it with grating couplers [6,11,13–15]; alternatively, they could exploit multiplane [9,10] or other mode separation techniques like a photonic lantern [16] as a fixed "front-end" preprocessor that transforms from large overlapping continuous spatial modes to the multiple discrete waveguide mesh inputs, allowing use of the technique with an arbitrary choice of modal basis.

Many sophisticated mesh networks of interferometers have been demonstrated that can work efficiently with complex multimode optical fields to provide linear operations [3–5, 11,15,17–29]. Several architectures offer self-configuration [6,11,13–15,30–33], with the simplest being a self-aligning beam coupler architecture [13], which is at the core of this paper; this can take an arbitrary set of (mutually coherent) inputs in a set of waveguides and deliver all the power to just one output waveguide. This self-configuration is based on a progressive set of simple one-parameter feedback loops to set the values of the various phase shifters and/or coupling elements in the mesh based on detected powers and without any calculations. In the automatic calibration process, we can also "calibrate out" the phase behavior of any "front-end" optics used to interface the mesh to the external optical world. A key point in this approach is that both the required calibration and the self-configuration and measurement could be completely automated using simple progressive algorithms and control circuits followed by elementary arithmetic calculations.

Though any optical component may have some losses due to imperfections, and any such waveguide systems are likely to have input coupling losses, otherwise these mesh analysis and generation schemes are perfectly efficient optically; there are no other power losses in the system, even for arbitrary (mutually coherent) inputs and/or outputs in the single-mode input or output waveguides in the meshes. Recent analysis suggests that such self-alignment can be accomplished in microseconds or shorter even when working with optical input powers of only ~10 μW per input [12] (given sufficiently fast adjustable phase shifters and/or couplers in the mesh). Hence, such an approach could be convenient, optically efficient, and fast.

In this paper, we discuss the approach of using self-configuring architectures for analyzing multimode beams in Section 2. In Section 3, we summarize the necessary general description of an MZI block. Section 4 shows how to deduce the input field from the self-configured mesh settings. Section 5 shows how to use the mesh as an arbitrary multimode generator. Calibration processes are summarized in Section 6. We draw conclusions in Section 7. Supporting detail is given in Supplement 1.

2. AUTOMATIC ANALYSIS OF A MULTIMODE BEAM

A. Self-Configuring Architectures

Two basic forms of self-configuring architectures of interferometers allow the self-aligning beam coupler [13]—those based on a "diagonal line" and those using a "binary tree" (see Fig. 1). Hybrids of these are also possible. (For completeness, the topology of such architectures is discussed in Supplement 1 Section S1, together with some other alternative architectures.) Each of the "diagonal line" and "binary tree" mesh architectures as shown here can be a "layer" of a general self-configuring architecture (Supplement 1 Section S1). Though we work here with only one such layer, multiple such layers can be cascaded for more complex functions, including arbitrary linear processors [14]. Each such layer consists of multiple "columns" of MZIs [34]. For the diagonal line, there is only one MZI per column, though in the binary tree there may be several in a given column.

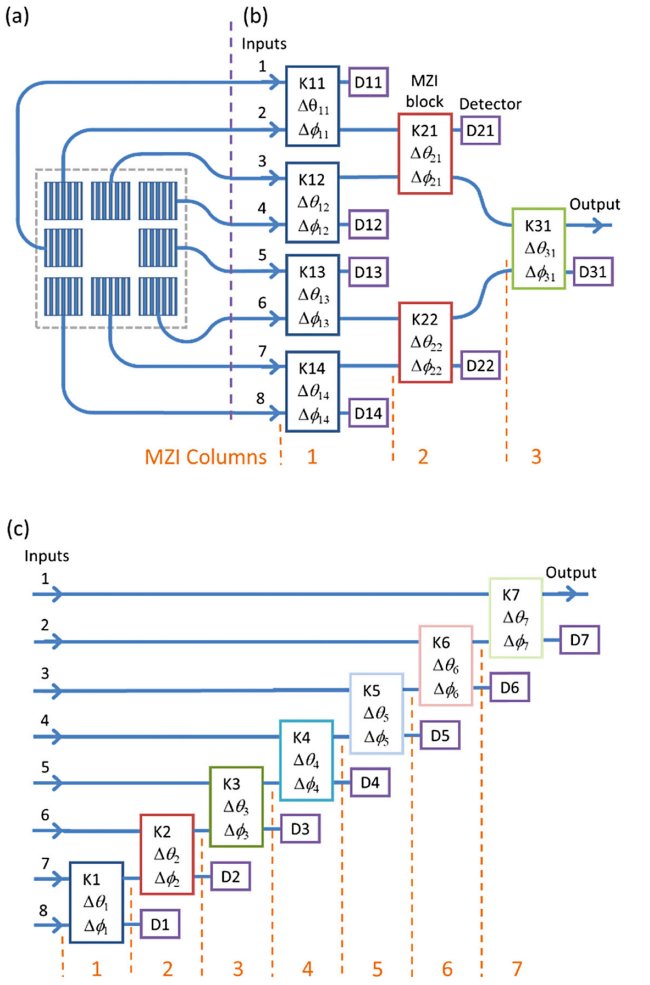

Fig. 1. Concept and architectures of a self-configuring mesh layer with optical inputs. (a) Example optical input, here with eight waveguides driven by the outputs from an example square array of grating couplers illuminated by some input light field. (b) Binary tree mesh, which we can self-configure to give all the resulting input power in the one output waveguide. Parameters $\Delta\theta$ and $\Delta\phi$ control the "split ratio" and one other phase shift in each 2×2 block K, respectively. Each such block can be implemented as an MZI. Elements D are detectors at the "drop ports" of these blocks or MZIs. (c) Alternative, diagonal line mesh architecture. The successive "columns" of MZIs are shown for both architectures.

For a "stand-alone" analyzer/generator, the binary tree may be preferable because (1) it allows some parallelization of the analysis process, (2) it is shorter—for N input or output waveguides, it requires only $\sim\log_2 N$ "columns" rather than the $\sim N-1$ "columns" of a diagonal line, and (3) all paths from the inputs to the output go through the same number of MZI and, hence, can have the same background loss. (Generally, background loss does not affect the functionality of the architectures and meshes here as long as it is equal on all paths; then, it just results in some uniform overall loss in the system. As a result, we will analyze our systems here as if they are lossless, with the understanding that there may be some such overall loss factor). The "diagonal line" approach may be preferable if we want to cascade multiple self-configuring layers (it can then lead to shorter architectures, without any crossing waveguides) and has the additional feature of being essentially symmetric from "front" to "back".

For mutually coherent light at the inputs, these architectures can self-configure to direct all the input power in the various input waveguides to the one output waveguide. This self-configuration can be achieved using a succession of single-parameter power minimizations at each of the "drop-port" detectors D11, D12, … or D1, D2, …. The self-configuring algorithms can be remarkably simple [13,14,31,33]. With the light field of interest shining on the optical inputs, the relative phase at the input to an MZI is adjusted first to minimize the "drop-port" power, then the "split ratio" of the MZI is adjusted to take that power to zero, and the MZIs are set this way in sequence starting with the MZI(s) in Column 1, proceeding through those in Column 2 and so on [13]. Multiple MZIs in a given column (as in the binary tree) can all be configured at the same time, in parallel (see [34] and Supplement 1 Section S1). It is also possible to self-configure the mesh based on power maximization just using a detector at the output (e.g., D31 or D7), though without the simple parallelization of the process in that case [13].

B. Analysis Algorithm and Modal Basis

The basic algorithm for using such a self-configuring layer to analyze a multimode beam is shown in Fig. 2(a). Once we have calibrated the mesh (see Section 6), we can shine in the optical field of interest, self-configure the mesh to route all the power to the output, and then deduce relative amplitudes and phases of the different parts or modes of the original beam from the resulting settings of the mesh. (The corresponding process for generating a desired output "backwards" from the inputs is shown in Fig. 2(b) and is discussed in Section 5).

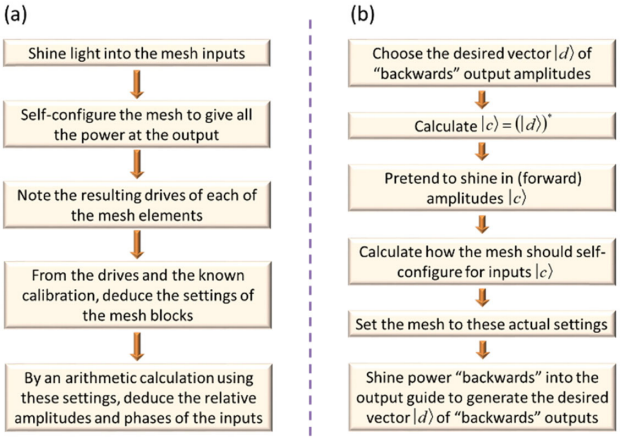

Fig. 2. Algorithm outlines (a) for automatic analysis of a multimode input field, (b) generating a desired "backwards" multimode output field.

Used directly with grating couplers as in Fig. 1(a), the "native" modes of this system corresponding to separate beams on the different grating couplers, each with the phase corresponding to the phase of the phase reference beam used in the system calibration (see Section 6) at the corresponding coupler; the modal analysis is done first on this basis.

If instead we use some fixed front-end mode transformer such as multiplane converters [9,10] or photonic lanterns [16] that deliver various different external (and likely overlapping) modes to different waveguide outputs that directly feed the inputs of the mesh, then those external modes become the effective modal basis on which this analysis is performed. Since the analyzer here has performed all the necessary physical interferometry, it is also possible in a simple mathematical calculation on those measured amplitude and phase values to transform the results after measurement to some other basis; essentially, we multiply the measured output vector of (complex) amplitudes by an appropriate unitary matrix U_B to change the modal basis for the measurement. That then means that the effective modal basis for the measurement is made up from specific different (and orthogonal) linear combinations (or input "vectors") of the input signals; indeed, the rows of the matrix U_B are then just the Hermitian adjoints (i.e., conjugate transpose) of those orthogonal input vectors. Hence, with this additional simple mathematical calculation (a matrix multiplication), this approach can be used to measure on any modal basis that is supported by the optics.

Now, we need to understand how the settings of an MZI relate to the input amplitudes and phases. So, we formally analyze the MZI (Section 3), and then deduce the expressions relating the settings to these field parameters (Section 4).

3. ANALYSIS OF MACH–ZEHNDER INTERFEROMETER

Here, we need a full form of the analysis of an MZI. We summarize this here, with necessary notations and with supporting detail in Supplement 1 Section S2.

Though only two phase shifters are required to give sufficient degrees of freedom in an MZI for it to function as a universal 2×2 block, for a general and flexible notation, we analyze it as if it has four phase shifters, as in Fig. 3(a). In use, we only need at least one phase shifter on at least one arm inside the MZI and any other one of these four phase shifters. We label the four ports of the MZI analogously to the four ports of a conceptual "cube"

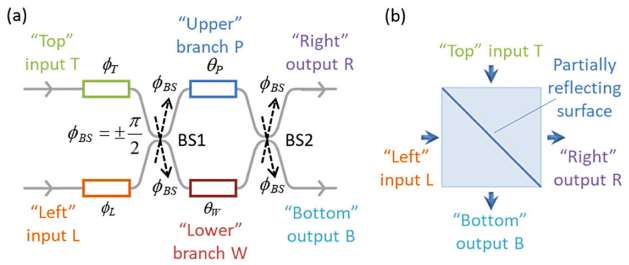

Fig. 3. (a) Schematic of a general waveguide MZI with up to four phase shifters (colored rectangles) on waveguides (gray lines), with two 50:50 beamsplitters BS1 and BS2, shown as directional couplers. (b) Corresponding conceptual BS showing "Top," "Left," "Bottom," and "Right" surfaces.

beam-splitter (BS) [Fig. 3(b)], as "Top" (T), "Left" (L), "Right" (R), and "Bottom" (B), with the notion that light can enter at the T port and be partially reflected to the R port, as well as partially transmitted to the B port, and similarly light incident in the L port will be partially reflected to the B port and partly transmitted to the R port. We also label the arms inside the interferometer as "Upper" (P) and "Lower" (W). The 50:50 waveguide BSs, BS1 and BS2, shown as directional couplers, couple light between the P and W waveguides to complete the MZI.

We need to define various phase delays, as shown in Fig. 3. We take ϕ_T to be the total phase delay from the "Top" input T, through the upper waveguide to the left end of the "Upper" branch phase shifter, marked with θ_P. Similarly, ϕ_L is the total phase delay lower waveguide from the "Left" input L to the left end of the "Lower" branch phase shifter marked with θ_W. θ_P and θ_W are similarly the total phase delays on the upper and lower waveguides, respectively, from the left ends of these "Upper" and "Lower" phase shifters, respectively, to the "Right" and "Bottom" output ports, respectively.

Note, there is necessarily an additional phase shift ϕ_{BS}, for light passing "through" the BSs from one waveguide to the other. (Our convention on phase shifts here is that a positive phase shift corresponds to a phase delay.) For a lossless BS (whether or not it has a 50:50 split), this phase shift is necessarily either $+\pi/2$ or $-\pi/2$ (within arbitrary additive multiples of 2π); this follows from power conservation (see Supplement 1 Section S3) and, hence, mathematical unitarity in a lossless system [14,35]. Whether the sign is "+" or "−" depends on the specifics of the BS (see Supplement 1 Section S4). For a directional coupler BS in a "first-order" design (i.e., with the shortest length for a given coupling to the "other" guide), this is a phase delay $+\pi/2$ (i.e., for a beam starting in one guide, the beam coupled over into the "other" guide is delayed by 90° compared to the beam remaining in the original guide). For definiteness now, and because this is the most likely form of a BS anyway, we choose $\phi_{BS} = +\pi/2$. (Note, incidentally, that for any such "shortest" directional coupler BS, even if it does not have a 50:50 BS ratio, this phase shift is still $+\pi/2$. Only if we lengthen the coupler so much that it moves into "second-order" behavior—coupling "over" and partially "back" again—does this number change to $-\pi/2$ or equivalently $+3\pi/2$.)

Though we will be physically controlling phase shifts such as ϕ_T, ϕ_L, θ_P, and/or θ_W—for example, a common approach is to control just the ϕ_T and θ_P phase shifters—the description of the MZI factorizes most simply using other resulting phases. For the two interferometer arms, we can usefully define the "common mode"

$$\theta_{av} = \frac{\theta_P + \theta_W}{2} \tag{1}$$

and "differential"

$$\Delta\theta = \theta_P - \theta_W \tag{2}$$

phase shifts. Similarly, for the input arms, we have "common mode"

$$\phi_{av} = \frac{\phi_T + \phi_L}{2} \tag{3}$$

and "differential"

$$\Delta\phi = \phi_T - \phi_L \tag{4}$$

phase shifts. We can also usefully define an overall phase shift from these:

$$\phi_{Tot} = \phi_{av} + \theta_{av} + \frac{\pi}{2} \tag{5}$$

(the inclusion of the additional $\pi/2$ makes later algebra simpler).

We can use the interference within an MZI to allow it to calibrate itself, in which case we calibrate these differential phases $\Delta\theta$ and $\Delta\phi$ (see Section 6) as a function of drive. We also have to know how we created these differential phase shifts—for example, by driving only the ϕ_T and θ_P phase shifters—so we can calculate the corresponding change in ϕ_{Tot} from Eqs. (1), (3), and (5) that is associated with any chosen setting of $\Delta\theta$ and $\Delta\phi$.

With input (complex) amplitudes a_T and a_L, respectively, for the propagating modes in the T and L input waveguides, leading to resulting propagating mode amplitudes a_R and a_B of the beams exiting in the R and B output waveguides, as derived in Supplement 1 Section S2, we can write the relation between inputs and outputs generally as

$$\begin{bmatrix} a_R \\ a_B \end{bmatrix} = \mathsf{M}\,(\phi_{Tot},\,\Delta\theta,\,\Delta\phi) \begin{bmatrix} a_T \\ a_L \end{bmatrix}. \tag{6}$$

Here, we are regarding the 2×2 matrix $\mathsf{M}(\phi_{Tot},\,\Delta\theta,\,\Delta\phi)$ for a given MZI as a function of ϕ_{Tot}, $\Delta\theta$, and $\Delta\phi$, which are themselves each functions of some of ϕ_T, ϕ_L, θ_P, and/or θ_W. This choice of matrix parameters also allows us factorize M as

$$\mathsf{M}(\phi_{Tot},\,\Delta\theta,\,\Delta\phi) = \exp\,(i\phi_{Tot})\,\mathsf{M}_s\,(\Delta\theta)\,\mathsf{M}_\phi\,(\Delta\phi)\,, \tag{7}$$

with

$$\mathsf{M}_\phi(\Delta\phi) = \begin{bmatrix} \exp\left(i\frac{\Delta\phi}{2}\right) & 0 \\ 0 & \exp\left(-i\frac{\Delta\phi}{2}\right) \end{bmatrix}. \tag{8}$$

For the simplest (and desired) case of 50:50 BSs, we obtain

$$\mathsf{M}_s\,(\Delta\theta) = \begin{bmatrix} \sin\left(\frac{\Delta\theta}{2}\right) & \cos\left(\frac{\Delta\theta}{2}\right) \\ \cos\left(\frac{\Delta\theta}{2}\right) & -\sin\left(\frac{\Delta\theta}{2}\right) \end{bmatrix}. \tag{9}$$

The full form of $\mathsf{M}_\phi(\Delta\phi)$ for other BS ratios is given in Eq. (S7) in Supplement 1 Section S2.

For use of the mesh as a generator, we need to run it "backwards" (i.e., shining light backwards into the R and/or B ports to have light emerge from the T and/or L ports). Then, by Eq. (S58) of Supplement 1 Section S5, the resulting matrix B in this direction is just the transpose of M (i.e., M^T). (We also want this backwards matrix B when performing the calculations to analyze an input field.) Given the specific factorization of Eq. (7) and these matrix symmetries, then the "backwards" matrix is

$$\begin{aligned}\mathsf{B}(\phi_{Tot},\,\Delta\theta,\,\Delta\phi) &= \mathsf{M}^T\,(\phi_{Tot},\,\Delta\theta,\,\Delta\phi) \\ &= \exp\,(i\phi_{Tot})\,\mathsf{M}_\phi^T\,(\Delta\phi)\,\mathsf{M}_s^T\,(\Delta\theta),\end{aligned} \tag{10}$$

where we note that the order of the matrix product in Eq. (10) has been inverted compared to that of Eq. (7) as a consequence of the transpose of the matrix product inverting the product order. {Matrix M_ϕ [Eq. (8)] is symmetric, so it is its own transpose, but we keep the transpose notation for similarity with later Hermitian adjoint algebra. Though M_s [Eq. (9)] is also symmetric for this ideal 50:50 BS case, in general, it is not [see Eq. (S7) in Supplement 1 Section S2], so we retain the explicit transpose for it also.}

So, with amplitudes b_R and b_B of backwards waves entering the R and B ports, respectively, and b_T and b_L emerging from the T and L ports, respectively, we have formally

$$\begin{bmatrix} b_T \\ b_L \end{bmatrix} = \mathsf{B}(\phi_{Tot}, \Delta\theta, \Delta\phi) \begin{bmatrix} b_R \\ b_B \end{bmatrix}, \tag{11}$$

with B as in Eq. (10).

4. DEDUCING THE INPUT VECTOR FROM THE MACH–ZEHNDER SETTINGS

Suppose, then, that we had shone the input vector $|c\rangle = [\, c_1 \; c_2 \; \ldots \; c_N \,]^T$ of complex amplitudes into the N input waveguides on the L in Fig. 1. (Here and below, we can use the Dirac notation $|c\rangle$ as a shorthand for such a column vector of complex amplitudes). Our approach to analyzing the relative amplitudes and phases of all these input forward amplitudes, Fig. 2(a), involves having the mesh self-configure so that, for such an input vector, all of the power appears in the single "Output" waveguide [at the R output of the MZI in the last column of the self-configuring layer, as in Figs. 1(b) or 1(c)]. Then, from the settings we now have in the MZIs, we wish to deduce the input vector $|c\rangle$ that led to these settings.

One simple way to envisage this calculation of $|c\rangle$ from the resulting mesh settings is to imagine that, with the mesh set this way, we now run the mesh backwards, shining (unit amplitude) light backwards into this Output waveguide. Then, we calculate the vector $|d\rangle \equiv [\, d_1 \; d_2 \; \ldots \; d_N \,]^T$ that would emerge "backwards" from the input guides. Then, by the phase-conjugating property of unitary meshes running backwards (Supplement 1 Section S5), and noting that a backwards-propagating beam in a single-mode guide is just the phase conjugate of a forward-propagating beam in that guide, we deduce

$$|c\rangle \equiv \left[\, c_1 \; c_2 \; \ldots \; c_N \,\right]^T = \left(\left[\, d_1 \; d_2 \; \ldots \; d_N \,\right]^T\right)^* \equiv (|d\rangle)^*, \tag{12}$$

completing the analysis of the input beam relative amplitudes and phases. In other words, the input vector $|c\rangle$ of amplitudes we calculate this way must have been the input vector of amplitudes that self-configured the mesh to these settings.

So, for each MZI, we can note that the drives that we are applying to the phase shifters are a result of the self-configuration process. Hence, using our presumed known calibration of the mesh elements, we can deduce the corresponding settings $\Delta\theta$ and $\Delta\phi$ that the self-configuration has set for this MZI. Again, knowing how we had driven the mesh phase shifters (i.e., what specific ones or combinations of ϕ_T, ϕ_L, θ_P, and/or θ_W we actually drove in calibration and in self-configuration and what drives we had applied), we can also now calculate the change in ϕ_{Tot} from Eqs. (1), (3), and (5). (We will already have compensated for any fixed phases implicit in ϕ_{Tot} as part of our phase calibration process, so such a change is all we need to know—see the discussion of calibration below in Section 6). Hence, we can calculate the corresponding matrix M as in Eq. (7) for each MZI, or, more usefully here, the corresponding "backwards" matrix B as in Eq. (10).

We can always construct a full $N \times N$ matrix for any mesh with N inputs and N outputs by progressively multiplying together the various 2×2 matrices for each block. Doing this appropriately for the backwards matrices B, we could calculate the corresponding $N \times N$ backwards matrix for the mesh, and we could perform calculations with that matrix. For our situation, though, we are only interested in calculating the backwards field at the "input" ports for hypothetical light in just one "output" port. As a consequence, we can set up the result even more simply and directly. We can write for each MZI

$$\mathsf{B} = \begin{bmatrix} \alpha & \mu \\ \beta & \nu \end{bmatrix}, \tag{13}$$

where we know all of these elements α, β, μ, and ν from the calculation using Eq. (10) for each block. Then, we start with a hypothetical backwards "input" vector in the block in the last column (e.g., block K31 or K7 in Fig. 1) with $b_R = 1$ and $b_B = 0$, (a vector $[\, 1 \; 0 \,]^T$) corresponding to shining hypothetical unit field backwards into the appropriate Output waveguide in Fig. 1. We can then simply work progressively "backwards" to the input, allowing us to write explicit expressions for each input waveguide amplitude. For this discussion, we subscript the α, β, μ, and ν in each block with the corresponding block number.

For example, for the binary tree mesh in Fig. 1(b), working backwards from the output, the backwards output vector at the left ports of K31 is $[\, \alpha_{31} \; \beta_{31} \,]^T$, so the backwards amplitude in the top left port of K31 is α_{31}. That then feeds the bottom right port of block K21, giving a backwards "input" vector at the right of block K21 of $[\, 0 \; \alpha_{31} \,]^T$, so the output backwards amplitude at the top left port of block K21 is $\mu_{21}\alpha_{31}$. Continuing similarly backwards through block K11, the top left output amplitude is $\mu_{11}\mu_{21}\alpha_{31}$. So, proceeding similarly for the various other backwards paths, we have explicitly for an eight-input mesh as in Fig. 1,

$$|d\rangle \equiv \begin{bmatrix} d_1 \\ d_2 \\ d_3 \\ d_4 \\ d_5 \\ d_6 \\ d_7 \\ d_8 \end{bmatrix} = \begin{bmatrix} \mu_{11}\mu_{21}\alpha_{31} \\ \nu_{11}\mu_{21}\alpha_{31} \\ \alpha_{12}\nu_{21}\alpha_{31} \\ \beta_{12}\nu_{21}\alpha_{31} \\ \mu_{13}\alpha_{22}\beta_{31} \\ \nu_{13}\alpha_{22}\beta_{31} \\ \alpha_{14}\beta_{22}\beta_{31} \\ \beta_{14}\beta_{22}\beta_{31} \end{bmatrix}. \tag{14}$$

So, explicitly again for such an eight-input binary tree mesh, we would conclude that the relative amplitudes and phases of the input beams in the eight input waveguides as used for the self-configuration must have been

$$|c\rangle \equiv \begin{bmatrix} c_1 \\ c_2 \\ c_3 \\ c_4 \\ c_5 \\ c_6 \\ c_7 \\ c_8 \end{bmatrix} = \begin{bmatrix} (\mu_{11}\mu_{21}\alpha_{31})^* \\ (\nu_{11}\mu_{21}\alpha_{31})^* \\ (\alpha_{12}\nu_{21}\alpha_{31})^* \\ (\beta_{12}\nu_{21}\alpha_{31})^* \\ (\mu_{13}\alpha_{22}\beta_{31})^* \\ (\nu_{13}\alpha_{22}\beta_{31})^* \\ (\alpha_{14}\beta_{22}\beta_{31})^* \\ (\beta_{14}\beta_{22}\beta_{31})^* \end{bmatrix} \equiv (|d\rangle)^*, \tag{15}$$

formally completing the analysis of the multimode input field. This process is easily extended for larger meshes (e.g., 16×1, 32×1, etc.). So, from the knowledge of how each MZI has been set in the self-configuration process with input amplitudes as in $|c\rangle$, we can calculate all the α, β, μ, and ν matrix elements for each block and, hence, deduce from Eq. (15) what the original input vector of field mode amplitudes $|c\rangle$—the one used to self-configure the mesh—actually was.

Note that this approach works for any of the choices of the pair of phase shifters (i.e., two phase shifters out of the four, of which at least one is on an MZI internal arm). (If we use only the phase shifters on the MZI internal arms, we need additional phase shifters on at least one input to each MZI in the "input" column (Column 3 in the example of Fig. 1), and the common-mode phase shifts in MZIs in one column end up performing the equivalent of the functions of the ϕ_T and ϕ_L phase shifters in the next column to the R).

For the eight-input diagonal line mesh as in Fig. 1(c), the corresponding result for $|c\rangle$ is, similarly,

$$|c\rangle = \begin{bmatrix} (\alpha_7)^* \\ (\alpha_6\beta_7)^* \\ (\alpha_5\beta_6\beta_7)^* \\ (\alpha_4\beta_5\beta_6\beta_7)^* \\ (\alpha_3\beta_4\beta_5\beta_6\beta_7)^* \\ (\alpha_2\beta_3\beta_4\beta_5\beta_6\beta_7)^* \\ (\alpha_1\beta_2\beta_3\beta_4\beta_5\beta_6\beta_7)^* \\ (\beta_1\beta_2\beta_3\beta_4\beta_5\beta_6\beta_7)^* \end{bmatrix}. \tag{16}$$

5. RUNNING THE MESH AS A GENERATOR

With a calibrated mesh, it is also straightforward to run the mesh in reverse, starting with actual light power fed backwards into the Output port as in Fig. 1 and using the mesh as a generator of any specific vector $|d\rangle$ of complex amplitudes emerging backwards from the "inputs" of the mesh. The algorithm is summarized briefly in Fig. 2(b).

To understand how to set the various drives in the mesh to generate some such "backwards" output vector, we can imagine we are configuring the mesh to take a vector $|c\rangle \equiv (|d\rangle)^*$ being shone into the mesh inputs in the forward direction to hypothetically put all the power in the output waveguide. If we set the mesh as if it was "collecting" this forward vector $|c\rangle$, then when run in the backwards direction, it will generate the desired vector $|d\rangle$ of outputs from the "input" ports. We give explicit details for the calculations of the required mesh parameters in Supplement 1 Section S6.

Note that, if we are using the mesh as a generator when operating with some additional "front-end" optics, such as such as multiplane converters [9,10] or photonic lanterns [16], it is important that, in that external optics, the loss is the same for all modes; otherwise, the whole system is not unitary within some overall loss factor, and the phase-conjugating property of unitary networks run backwards does not apply. Then, running the whole system backwards as a generator would not lead to the desired backwards output; it would not be the phase conjugate of the hypothetical forward vector $|c\rangle$ of modal amplitudes at the front end of the entire optical system.

6. CALIBRATION

When working with complex meshes in applications such as these, it is essential that the mesh and its elements are calibrated. There are two aspects to the calibration: (i) "split ratio" (or $\Delta\theta$) calibration of the MZIs; and (ii) phase (or $\Delta\phi$) calibration. It is obviously useful that such calibration is simple and automatic.

In calibrating the phase in the system, we need to choose an external phase reference of some kind. That could be just some flat phase front shining directly into the waveguides of the integrated optics, but, more generally, it could be a phase reference such as a plane wave, or light from some point source, shining into some external front-end optics. That external optics could include lenses, optical fibers, or mode converters such as photonic lanterns or multiplane light converters in front of the integrated photonic mesh.

Integrated optical systems may hold a relatively stable phase calibration (especially if care is taken to make physical path lengths essentially equal for all beams that must interfere). In external optics, however, phase delays may well drift significantly with temperature or time. Furthermore, we may want to make changes to the front-end optics, such as changing focusing or even the modal decomposition basis of a complex system like a multiplane light converter. So, calibrating to that external phase reference also means we can "calibrate out" all the static phase behavior of such front-end optics and can recalibrate for any changes in that phase behavior. Note, though, that, because the mesh must be configured in specific ways to perform the calibration, the calibration cannot be run at the same time as the system is operating to measure or generate fields.

In operation, for each MZI, we will have some drive v_θ (e.g., a voltage) that we are using to adjust $\Delta\theta$, and similarly some drive v_ϕ that we are using to adjust $\Delta\phi$. For example, v_θ might be the voltage used to drive a θ_P phase shifter, and, similarly, v_ϕ might be the drive voltage for a ϕ_T phase shifter. Calibrating means deducing the functions $\Delta\theta(v_\theta)$ and $\Delta\phi(v_\phi)$ (e.g., based on "look-up" tables of specific calibrated values) for each MZI. We use the functions $\Delta\theta(v_\theta)$ and $\Delta\phi(v_\phi)$ directly if we are running the mesh as a multimode analyzer so that we can deduce the $\Delta\theta$ and $\Delta\phi$ values for each MZI from the v_θ and v_ϕ values that have been set in the self-configuration. For running the mesh as a multimode generator, we can then numerically invert these calibration functions $\Delta\theta(v_\theta)$ and $\Delta\phi(v_\phi)$ to get functions $v_\theta(\Delta\theta)$ and $v_\phi(\Delta\phi)$ for each MZI; these tell us what drives v_θ and v_ϕ to apply to get the desired $\Delta\theta$ and $\Delta\phi$ in each MZI. We start with the calibration of the $\Delta\theta$ for each MZI and then move on to calibrating their $\Delta\phi$ behavior. We give detailed calibration procedures and formulas in Supplement 1 Section S7, but we can summarize the overall approach here (Fig. 4).

The first part of the calibration is to calibrate the $\Delta\theta(v_\theta)$ function for each MZI. We do this by arranging optically that there is input power in just one of the two input ports (e.g., the T port)

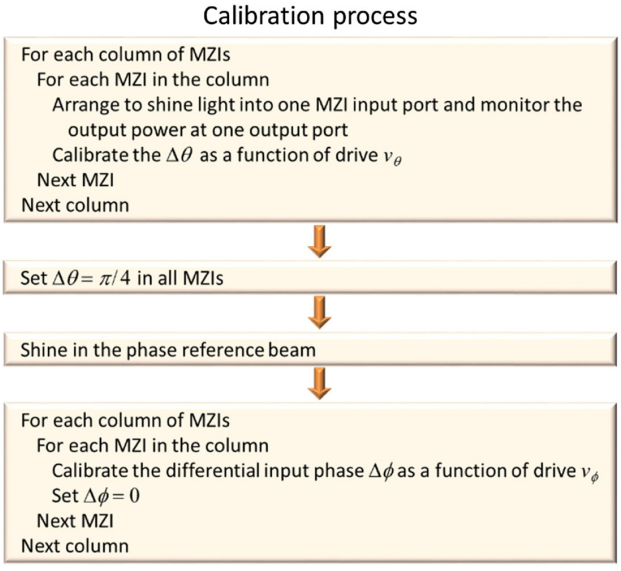

Fig. 4. Outline of the calibration process.

of a given MZI. Then, we use what we can call a "co-sinusoidal proportional calibration" to deduce $\Delta\theta(v_\theta)$ as we vary v_θ; this is a relatively standard approach, though specifically this version is done using measured minimum and maximum output powers rather than presuming a minimum power of zero.

We can arrange for such an input power at just one port of an MZI in the mesh either in a "forwards" or "backwards" $\Delta\theta$ calibration approach. In a "forwards" calibration of the mesh, we require the input calibration power to be controllably in only one input port of the mesh at a time. Detectors for the calibration can be on the "drop ports" of the MZI, or we can use just the overall output power in the mesh output waveguide (though then the calibration of different MZIs cannot be "parallelized"). In a "backwards" calibration, we instead shine just one fixed backwards beam into the "output" of the mesh, but we need to be able to monitor the power emerging backwards from the inputs to perform the calibration. In both schemes, we proceed through the MZIs in a corresponding "forwards" or "backwards" sequence. (For a diagonal line self-configuring layer, because it is essentially symmetric from front to back, we can also run a "forwards" $\Delta\theta$ calibration with a single source, in a manner analogous to the "backwards" sequence here. See also [33].)

Having calibrated $\Delta\theta(v_\theta)$ for each MZI, to calibrate the $\Delta\phi(v_\phi)$ function for each MZI, essentially we set all the MZIs to $\Delta\theta = \pi/4$ (so the MZIs are each behaving like 50:50 BSs overall). Then, we shine in a "phase reference" beam over all the inputs; as discussed above, this phase reference can be one that is "in front of" any front-end optics. Using this reference, we then calibrate $\Delta\phi(v_\phi)$ for each MZI. By using the "co-sinusoidal proportional calibration" approach, importantly, we do not have to have equal input powers on the two ports of a given MZI; hence, for this calibration, essentially only the phase "shape" of that phase reference beam matters, not its intensity "shape". We work from the input MZIs progressively "forwards" through successive columns, starting from the "input" column; in each case, we set $\Delta\phi = 0$ in a given MZI once we have calibrated it. Note that this $\Delta\phi$ calibration only works perfectly if the BSs in the MZI have quite an accurate 50:50 splitting ratio (see Supplement 1 Section S7). If attaining such accurate splitting is not reliable in fabrication, then we could take the "double-MZI" approach as in [31,32], which can compensate such imperfections at the expense of some greater circuit complexity. Such an approach would also allow us to readjust the effective splitting ratios to allow us to work at different specific wavelengths.

This phase calibration approach, including setting all MZIs in "earlier" columns to $\Delta\phi = 0$ as we proceed to calibrate those in "later" columns, also means we automatically "calibrate out" any fixed phase delays in the system. Equivalently, it means that, for analysis or generation, we can proceed for each MZI as if

$$\phi_{\mathrm{av}} = 0 \quad \text{if } \Delta\phi = 0 \quad \text{and} \quad \theta_{\mathrm{av}} = 0 \quad \text{if } \Delta\theta = 0. \tag{17}$$

Of course, if we change any of ϕ_{T}, ϕ_{L}, θ_{P}, and/or θ_{W} in use, and we certainly will as we set $\Delta\theta$ and $\Delta\phi$ for given MZIs, we will change θ_{av} and ϕ_{av} by known amounts as a result, and we have to include that in our overall calculations, but we can start from the simple "baseline" as given by Eq. (17). For example, if we are using the ϕ_{T} and θ_{P} phase shifters to adjust the MZI, then, starting from this calibration and using Eqs. (1)–(5),

$$\Delta\theta = \theta_{\mathrm{P}},\ \Delta\phi = \phi_{\mathrm{T}},\ \phi_{\mathrm{Tot}} = \phi_{\mathrm{av}} + \theta_{\mathrm{av}} + \frac{\pi}{2} = \frac{\phi_{\mathrm{T}}}{2} + \frac{\theta_{\mathrm{P}}}{2} + \frac{\pi}{2}, \tag{18}$$

and we will use these relations when calculating the overall matrix $\mathbf{M}$ for a given MZI from Eq. (7).

There will obviously still be an additional overall phase delay in propagating through the system, but it will be the same for all paths, at least within additive multiples of 2π, and hence does not matter for the purposes of multimode generation or analysis, where we only care about relative phases and amplitudes in the corresponding outputs or inputs.

Incidentally, if we want to calibrate a system with multiple self-configuring "layers" (see Supplement 1 Section S1), then we use a similar overall calibration process as we proceed to calibrate the "next" (and any subsequent) self-configuring layer(s). Specifically, we will set all blocks in preceding layers to $\Delta\phi = 0$ when we shine in the external phase reference. A later layer then treats all preceding layers as if they are just some extended "front-end" optics as we calibrate to that external phase reference.

One important point in both the calibration and operation of these networks is that we are presuming that cross talk between the settings of the elements is negligible; otherwise, we are not able to adjust one element without unintentionally affecting another element. In the engineering of such systems, it will be important to minimize any such effects, such as thermal cross talk [36].

Hence, we can have a straightforward and progressive calibration approach that could be completely automated. If we use the "backwards" $\Delta\theta(v_\theta)$ calibration, the calibration of the entire mesh can be accomplished with just two optical beams—one "backwards" power beam in the output waveguide for the $\Delta\theta(v_\theta)$ calibration and one "forwards" phase reference beam for the $\Delta\phi(v_\phi)$ calibration.

7. CONCLUSIONS

We have shown that there is a simple, automatic method for analyzing the full amplitude and phase of the components of a multimode optical field and for generating any such field on a given modal basis. Effectively, in one automatic process, we perform all the necessary interferometry in a mesh of two-beam interferometers. This process may be fast enough to measure such multimode fields in real time, e.g., on microsecond time scales.

We also show how this system can be calibrated automatically. Importantly, all these processes require only simple sequential algorithms and arithmetic calculations, based physically on power minimization or maximization in photodetectors as we adjust each parameter one by one. As presented here, these approaches presume "perfect" components, with balanced losses and path lengths, and neglecting other potential problems such as back-reflections, thermal and optical cross talk, and limited resolution in setting element properties. Though some imperfections such as imperfect BS coupling ratios could be compensated, e.g., using "double-MZI" techniques [32,33], the effect of imperfections merits future investigation. Nonetheless, this approach gives a starting point and offers a simple and fast method for full analysis and arbitrary generation of multimode fields in optics, for potential applications in communications, processing, and sensing of various kinds.

Funding. Air Force Office of Scientific Research (FA9550-17-1-0002).

Acknowledgment. I thank Sunil Pai for many stimulating discussions.

Disclosures. The author declares no conflict of interest.

See Supplement 1 for supporting content.

REFERENCES

1. D. A. B. Miller, "Waves, modes, communications, and optics: a tutorial," Adv. Opt. Photon. **11**, 679–825 (2019).
2. P. J. Winzer, D. T. Neilson, and A. R. Chraplyvy, "Fiber-optic transmission and networking: the previous 20 and the next 20 years [Invited]," Opt. Express **26**, 24190–24239 (2018).
3. J. Carolan, C. Harrold, C. Sparrow, E. Martín-López, N. J. Russell, J. W. Silverstone, P. J. Shadbolt, N. Matsuda, M. Oguma, M. Itoh, G. D. Marshall, M. G. Thompson, J. C. F. Matthews, T. Hashimoto, J. L. O'Brien, and A. Laing, "Universal linear optics," Science **349**, 711–716 (2015).
4. N. C. Harris, J. Carolan, D. Bunandar, M. Prabhu, M. Hochberg, T. Baehr-Jones, M. L. Fanto, A. M. Smith, C. C. Tison, P. M. Alsing, and D. Englund, "Linear programmable nanophotonic processors," Optica **5**, 1623–1631 (2018).
5. D. Pérez, I. Gasulla, and J. Capmany, "Programmable multifunctional integrated nanophotonics," Nanophotonics **7**, 1351–1371 (2018).
6. D. A. B. Miller, "Establishing optimal wave communication channels automatically," J. Lightwave Technol. **31**, 3987–3994 (2013).
7. S. M. Popoff, G. Lerosey, R. Carminati, M. Fink, A. C. Boccara, and S. Gigan, "Measuring the transmission matrix in optics: an approach to the study and control of light propagation in disordered media," Phys. Rev. Lett. **104**, 100601 (2010).
8. J. Carpenter, B. J. Eggleton, and J. Schröder, "Complete spatiotemporal characterization and optical transfer matrix inversion of a 420 mode fiber," Opt. Lett. **41**, 5580–5583 (2016).
9. N. K. Fontaine, R. Ryf, H. Chen, D. T. Neilson, K. Kim, and J. Carpenter, "Laguerre–Gaussian mode sorter," Nat. Commun. **10**, 1865 (2019).
10. G. Labroille, B. Denolle, P. Jian, P. Genevaux, N. Treps, and J.-F. Morizur, "Efficient and mode selective spatial mode multiplexer based on multi-plane light conversion," Opt. Express **22**, 15599–15607 (2014).
11. A. Annoni, E. Guglielmi, M. Carminati, G. Ferrari, M. Sampietro, D. A. B. Miller, A. Melloni, and F. Morichetti, "Unscrambling light–automatically undoing strong mixing between modes," Light Sci. Appl. **6**, e17110 (2017).
12. K. Choutagunta, I. Roberts, D. A. B. Miller, and J. M. Kahn, "Adapting Mach–Zehnder mesh equalizers in direct-detection mode-division-multiplexed links," J. Lightwave Technol. **38**, 723–735 (2020).
13. D. A. B. Miller, "Self-aligning universal beam coupler," Opt. Express **21**, 6360–6370 (2013).
14. D. A. B. Miller, "Self-configuring universal linear optical component," Photon. Res. **1**, 1–15 (2013).
15. A. Ribeiro, A. Ruocco, L. Vanacker, and W. Bogaerts, "Demonstration of a 4×4-port universal linear circuit," Optica **3**, 1348–1357 (2016).
16. T. A. Birks, I. Gris-Sánchez, S. Yerolatsitis, S. G. Leon-Saval, and R. R. Thomson, "The photonic lantern," Adv. Opt. Photon. **7**, 107–167 (2015).
17. Y. Shen, N. C. Harris, S. Skirlo, M. Prabhu, T. Baehr-Jones, M. Hochberg, X. Sun, S. Zhao, H. Larochelle, D. Englund, and M. Soljacic, "Deep learning with coherent nanophotonic circuits," Nat. Photonics **11**, 441–446 (2017).
18. N. C. Harris, G. R. Steinbrecher, J. Mower, Y. Lahini, M. Prabhu, D. Bunandar, C. Chen, F. N. C. Wong, T. Baehr-Jones, M. Hochberg, S. Lloyd, and D. Englund, "Quantum transport simulations in a programmable nanophotonic processor," Nat. Photonics **11**, 447–452 (2017).
19. P. L. Mennea, W. R. Clements, D. H. Smith, J. C. Gates, B. J. Metcalf, R. H. S. Bannerman, R. Burgwal, J. J. Renema, W. S. Kolthammer, I. A. Walmsley, and P. G. R. Smith, "Modular linear optical circuits," Optica **5**, 1087–1090 (2018).
20. X. Qiang, X. Zhou, J. Wang, C. M. Wilkes, T. Loke, S. O'Gara, L. Kling, G. D. Marshall, R. Santagati, T. C. Ralph, J. B. Wang, J. L. O'Brien, M. G. Thompson, and J. C. F. Matthews, "Large-scale silicon quantum photonics implementing arbitrary two-qubit processing," Nat. Photonics **12**, 534–539 (2018).
21. J. Wang, S. Paesani, Y. Ding, R. Santagati, P. Skrzypczyk, A. Salavrakos, J. Tura, R. Augusiak, L. Mančinska, D. Bacco, D. Bonneau, J. W. Silverstone, Q. Gong, A. Acín, K. Rottwitt, L. K. Oxenløwe, J. L. O'Brien, A. Laing, and M. G. Thompson, "Multidimensional quantum entanglement with large-scale integrated optics," Science **360**, 285–291 (2018).
22. I. V. Dyakonov, I. A. Pogorelov, I. B. Bobrov, A. A. Kalinkin, S. S. Straupe, S. P. Kulik, P. V. Dyakonov, and S. A. Evlashin, "Reconfigurable photonics on a glass chip," Phys. Rev. Appl. **10**, 044048 (2018).
23. F. Shokraneh, S. Geoffroy-Gagnon, M. Sanadgol Nezami, and O. Liboiron-Ladouceur, "A single layer neural network implemented by a 4×4 MZI-based optical processor," IEEE Photon. J. **11**, 4501612 (2019).
24. C. Taballione, T. A. W. Wolterink, J. Lugani, A. Eckstein, B. A. Bell, R. Grootjans, I. Visscher, D. Geskus, C. G. H. Roeloffzen, J. J. Renema, I. A. Walmsley, P. W. H. Pinkse, and K.-J. Boller, "8×8 reconfigurable quantum photonic processor based on silicon nitride waveguides," Opt. Express **27**, 26842–26857 (2019).
25. L. Zhuang, C. G. H. Roeloffzen, M. Hoekman, K.-J. Boller, and A. J. Lowery, "Programmable photonic signal processor chip for radiofrequency applications," Optica **2**, 854–859 (2015).
26. D. Perez, I. Gasulla, F. J. Fraile, L. Crudgington, D. J. Thomson, A. Z. Khokhar, K. Li, W. Cao, G. Z. Mashanovich, and J. Capmany, "Silicon photonics rectangular universal interferometer," Laser Photon. Rev. **11**, 1700219 (2017).
27. D. Pérez, I. Gasulla, and J. Capmany, "Field-programmable photonic arrays," Opt. Express **26**, 27265–27278 (2018).
28. D. Pérez, I. Gasulla, L. Crudgington, D. J. Thomson, A. Z. Khokhar, K. Li, W. Cao, G. Z. Mashanovich, and J. Capmany, "Multipurpose silicon photonics signal processor core," Nat. Commun. **8**, 636 (2017).
29. D. Pérez and J. Capmany, "Scalable analysis for arbitrary photonic integrated waveguide meshes," Optica **6**, 19–27 (2019).
30. D. A. B. Miller, "Reconfigurable add-drop multiplexer for spatial modes," Opt. Express **21**, 20220–20229 (2013).
31. D. A. B. Miller, "Perfect optics with imperfect components," Optica **2**, 747–750 (2015).
32. C. M. Wilkes, X. Qiang, J. Wang, R. Santagati, S. Paesani, X. Zhou, D. A. B. Miller, G. D. Marshall, M. G. Thompson, and J. L. O'Brien, "60 dB high-extinction auto-configured Mach–Zehnder interferometer," Opt. Lett. **41**, 5318–5321 (2016).
33. D. A. B. Miller, "Setting up meshes of interferometers–reversed local light interference method," Opt. Express **25**, 29233–29248 (2017).
34. S. Pai, I. A. D. Williamson, T. W. Hughes, M. Minkov, O. Solgaard, S. Fan, and D. A. B. Miller, "Parallel programming of an arbitrary feedforward photonic network," IEEE J. Sel. Topics Quantum Electron. (Early Access) (2020), 10.1109/JSTQE.2020.2997849.
35. R. Loudon, *Quantum Theory of Light*, 3rd ed. (Oxford, 2000), pp. 88–91.
36. M. Milanizadeh, D. Aguiar, A. Melloni, and F. Morichetti, "Canceling thermal cross-talk effects in photonic integrated circuits," J. Lightwave Technol. **37**, 1325–1332 (2019).